Casimir force, causality, and the Gurzhi model

G. L. Klimchitskaya, V. M. Mostepanenko, Kailiang Yu, and L. M. Woods

The Casimir force, causality and the Gurzhi model

G. L. Klimchitskaya,[1,2] V. M. Mostepanenko,[1,2,3] Kailiang Yu,[4] and L. M. Woods[4]

[1]*Central Astronomical Observatory at Pulkovo of the Russian*

Academy of Sciences, Saint Petersburg, 196140, Russia

[2]*Institute of Physics, Nanotechnology and Telecommunications,*

Peter the Great Saint Petersburg Polytechnic University, Saint Petersburg, 195251, Russia

[3]*Kazan Federal University, Kazan, 420008, Russia*

[4]*Department of Physics, University of South Florida, Tampa, Florida 33620, USA*

Abstract

An extended Drude model, termed as the Gurzhi model, which takes into account the electron-phonon and electron-electron interactions, is applied to calculate the Casimir force between two metallic plates. It is shown that although the dielectric permittivity of the Gurzhi model has a first order pole in the upper half-plane of complex frequencies and, thus, violates the causality principle, it can be used in a restricted frequency interval in combination with the experimental permittivity determined by the optical data for the complex index of refraction. The imaginary part of the Gurzhi dielectric permittivity of Au at low frequencies demonstrates better agreement with the permittivity given by the optical data than the simple Drude model. The Casimir pressure between two Au plates is computed using the Gurzhi, Drude and plasma model approaches, taking into account the optical data, as well as with the simple Drude and plasma models. The contribution of the electron-electron scattering to the Casimir pressure is estimated. Although a comparison with the measurement data of two precise experiments show that the Gurzhi model does not resolve the Casimir puzzle, the obtained results suggest further clarification of this fundamental problem.

I. INTRODUCTION

It is common knowledge that the zero-point and thermal fluctuations of the electromagnetic field are responsible for several interesting physical phenomena which attract much experimental and theoretical attention in the last few years. The best known example is the fluctuation-induced force acting between two closely spaced uncharged bodies in vacuum. At separations below a few nanometers one can neglect the presence of retardation and this force is known as the van der Waals force. At larger separations, where the effects of retardation come into play, it is conventional to speak about the Casimir force (see the recent reviews [1–3]). Theoretical description of the van der Waals and Casimir forces is given by the Lifshitz theory [4] which is derivable from the fluctuation-dissipation theorem of quantum statistical physics, or from the scattering approach, or by summing up the oscillator free energies in the framework of quantum field theory [5–8].

The Lifshitz theory allows computation of the van der Waals and Casimir energies, free energies and forces given the frequency-dependent dielectric permittivities of the interacting bodies are available. These permittivities are obtained from the complex index of refraction which has been measured for a number of materials over some frequency regions [9]. The characteristic feature of the van der Waals and Casimir forces is that their calculation requires a knowledge of the dielectric permittivities over very wide frequency regions including at zero frequency. The latter contributes significantly to the final result. Because of this, it is necessary to extrapolate the available optical data down to zero frequency on theoretical grounds. As an example, for metals extrapolations of this kind are usually made by means of the Drude model which takes into account the electron-phonon interaction at low frequencies. The physical significance and properties of the Drude model are discussed in detail in Ref. [10].

Surprisingly, in a number of experiments performed by two different groups [11–21] it was found that the measurement results exclude theoretical predictions of the Lifshitz theory obtained using an extrapolation of the optical data by means of the Drude model. The same results turned out to be in agreement with theory if the optical data reflecting the role of core (bound) electrons are extrapolated down to zero frequency by the free-electron plasma model [11–21]. An important role in these comparisons is played by the contribution of the zero-frequency term of the Lifshitz formula which depends heavily on the extrapolation used.

2

It seems quite unusual that the Lifshitz theory is excluded by the measurement data if the actual relaxation properties of conduction electrons at low frequencies are taken into account but it agrees with the data if these properties are disregarded. Taking into consideration that the difference between two alternative theoretical predictions at the experimental separations of Refs. [11–21] was below a few percent, attempts of solving the problem at the expense of some background effects or computational inaccuracies have been undertaken (see, e.g., Refs. [22–25]).

The experimental situation was finally cleared up employing the differential force measurements proposed in Ref. [26] where the theoretical predictions of the Lifshitz theory obtained with the help of the Drude- and plasma-model extrapolations of the optical data differ by up to a factor of 1000. The experiment of this kind [27] conclusively excluded an extrapolation by means of the Drude model and turned out to be in agreement with theoretical results using the plasma model.

A disagreement between theoretical predictions of the Lifshitz theory obtained using the physically justified Drude model and measurement results from many experiments is considered as puzzling [28]. The roots of the Casimir puzzle are directly related to the fact that according to the Drude model there is no contribution to the Casimir force from the transverse electric mode at zero frequency [29]. As a result, at large separations between the interacting plates the predicted Casimir force is only one half of the one predicted using the plasma model. The single experiment performed at large separations up to 7.3 micrometers [30] was interpreted as being in agreement with the Drude model prediction. In this experiment, however, not the Casimir force alone, but up to an order of magnitude larger force presumably originating from the so-called patch potentials was measured. The Casimir force itself was obtained indirectly using large subtraction of some analytic expression containing two fitting parameters. According to Refs. [31, 32], this makes the results of Ref. [30] uncertain. Various aspects of the Casimir puzzle are discussed at length in Refs. [1, 3, 8, 10, 21, 27, 28, 33–35].

Taking into account that a fundamental understanding of the Casimir puzzle is still missing, it seems warranted to reconsider the response of metals to the low-frequency electromagnetic field used in the Lifshitz theory. In the low frequency range, the electromagnetic response is determined by the intraband part which is essentially governed by the behavior of conduction electrons. Experimental studies using a variety of spectroscopic techniques show

3

that much insight can be gained in the band structure properties of the materials as well as the scattering processes carriers exhibit in their dynamics [36]. The relaxation parameter γ_{ep} of the standard Drude model is determined by the electron-phonon scattering. However, at low frequencies electron-electron, electron-impurity, electron-surface and other interactions contribute to the total relaxation parameter as well (see Ref. [37] and review [38]), where in clean metallic systems electron-electron scattering is the major addition to the electron-phonon one. It has been known that for noble metals the contribution of electron-electron scattering γ_{ee} to the relaxation parameter can be described by the Gurzhi formula [38–41] which contains both the frequency- and temperature-dependent terms. Replacing γ_{ep} in the dielectric permittivity of the Drude model with $\gamma_{ep} + \gamma_{ee}$, one obtains the so-called extended Drude, or Gurzhi model for the dielectric permittivity of metals.

In this paper, we investigate possible applications of the Gurzhi model in the Lifshitz theory for calculations of the Casimir force. We explore the analytic properties of the Gurzhi dielectric permittivity and demonstrate that it violates the causality condition which precludes its use over the entire frequency axis. Next, we consider the dielectric permittivities of the Gurzhi, Drude and plasma models in combination with the measured optical data. It is confirmed that over some frequency region below 2 eV the Gurzhi model provides a better analytic approximation to the measured imaginary part of the dielectric permittivity of Au than the Drude model. The Casimir pressure between two parallel plates made of Au is computed using the optical data extrapolated down to zero frequency by means of the Gurzhi, Drude and plasma models, and the obtained results are compared. This allowed estimation of the possible role of electron-electron interactions in the Casimir force. The Casimir pressures computed with different models of the dielectric permittivity are correlated with precise experiments on measuring the Casimir interaction. It is shown that although the Gurzhi model provides a better analytic approximation to the optical data in some frequency range than the Drude one, it does not resolve the Casimir puzzle.

The paper is organized as follows. In Sec. II we describe the main features of the Gurzhi model and consider its analytic properties in connection with the causality principle. Section III is devoted to comparison between different analytic models of the dielectric permittivity of Au combined with the measured optical data. In Sec. IV the Casimir interaction computed using different permittivities is compared with the measurement results of two precise experiments. In Sec. V the reader will find our conclusions and discussion.

II. THE GURZHI DIELECTRIC PERMITTIVITY AND ITS ANALYTIC PROPERTIES

It is well known that at sufficiently low frequencies the response of metals to electromagnetic field is essentially described by the dielectric permittivity of the Drude model

$$\varepsilon_D(\omega, T) = 1 - \frac{\omega_p^2}{\omega[\omega + i\gamma_{ep}(T)]}, \tag{1}$$

where ω_p is the plasma frequency and $\gamma_{ep}(T)$ is the temperature-dependent relaxation parameter determined by the process of electron-phonon scattering.

An extended version of the Drude dielectric permittivity, which is called sometimes the Gurzhi model, takes a similar form

$$\varepsilon_G(\omega, T) = 1 - \frac{\omega_p^2}{\omega[\omega + i\gamma(\omega, T)]}. \tag{2}$$

Here, however, the relaxation parameter consists of two terms

$$\gamma(\omega, T) = \gamma_{ep}(T) + \gamma_{ee}(\omega, T) \tag{3}$$

taking into account the processes of electron-phonon and electron-electron scattering.

The theoretical expression for γ_{ee} was derived in Ref. [39] (see also Refs. [38, 40, 41]) based on the Boltzmann quantum equation for the electronic Fermi liquid and the Kubo formula which relates the conductivity to the current-current correlation function

$$\gamma_{ee}(\omega, T) = D\left[(k_B T)^2 + \left(\frac{\hbar\omega}{2\pi}\right)^2\right]. \tag{4}$$

Here, the coefficient $D = \pi^3 \Gamma \Delta/(12\hbar E_F)$ where E_F is the Fermi level of the metal under consideration, k_B is the Boltzmann constant, $\Delta = 0.75$ is the fractional umklapp scattering, and $\Gamma = 0.55$ is the averaged scattering probability over the Fermi surface. Note that Eq. (4) has been verified in several experiments for noble metals [42–45] in the near infrared frequency range up to the interband absorption frequencies. In so doing, the temperature-dependent contribution in Eq. (4) is small as compared to the frequency-dependent one. For Au, which is the metal of our interest below, one has $D = 0.94$ fs^{-1}eV^{-2} [41].

Substituting Eq. (4) in Eq. (3), the relaxation parameter taking into account both the electron-phonon and electron-electron scattering can be written in the form

$$\gamma(\omega, T) = C(T) + B\omega^2, \tag{5}$$

5

where

$$C(T) = \gamma_{ep}(T) + D(k_B T)^2, \quad B = D\left(\frac{\hbar}{2\pi}\right)^2. \tag{6}$$

The dielectric permittivity of the Gurzhi model (2), (5), besides the singular point at $\omega = 0$, has poles in the plane of complex frequencies determined by the roots of the quantity

$$iB\omega^2 + \omega + iC(T) = 0. \tag{7}$$

By solving this equation, one obtains

$$\omega^{(1,2)} = i\xi^{(1,2)} = \frac{i}{2B}\left[1 \pm \sqrt{1 + 4BC(T)}\right], \tag{8}$$

where $\omega^{(1)}$ and $\omega^{(2)}$ belong to the upper and lower half-planes, respectively.

Along the imaginary frequency axis $\omega = i\xi$ the Gurzhi dielectric permittivity (2), (4) takes the real values

$$\varepsilon_G(i\xi) = 1 + \frac{\omega_p^2}{\xi\left[\xi + C(T) - B\xi^2\right]}. \tag{9}$$

As an example, in Fig. 1 ε_G is shown as a function of ξ for Au at room temperature using the parameters of the Gurzhi model indicated above and the experimental parameters of the Drude model $\hbar\omega_p = 8.68$ eV and $\hbar\gamma_{ep}(T = 295\,\mathrm{K}) = 30.3$ meV [41]. From Eq. (9) and Fig. 1 it is seen that the dielectric permittivity ε_G reaches the minimum value $\varepsilon_G(i\xi^{(m)}) = 1.1267$ at the point

$$\hbar\xi^{(m)} = \frac{\hbar}{3B}\left[1 + \sqrt{1 + 3BC(T)}\right] = 42.2094\,\mathrm{eV} \tag{10}$$

and has a break of continuity at the point $\hbar\xi^{(1)} = 63.3217$ eV defined in Eq. (8). It is important to note that in the region from $\hbar\xi^{(1)}$ to $\hbar\xi^{(0)} \approx 64.47$ eV the Gurzhi permittivity takes the negative values and vanishes at $\xi = \xi^{(0)}$: $\varepsilon_G(i\xi^{(0)}) = 0$. For $\xi > \xi^{(0)}$ ε_G increases monotonously and goes to unity when ξ goes to infinity.

These properties are not normal for commonly employed dielectric permittivities which must meet some necessary physical conditions. It has been known that the electric displacement $\boldsymbol{D}(t)$ is determined by the values of electric field $\boldsymbol{E}(t)$ at all *previous* moments of time [46]

$$\boldsymbol{D}(t) = \boldsymbol{E}(t) + \int_0^\infty f(\tau)\boldsymbol{E}(t - \tau)d\tau, \tag{11}$$

where the function of time $f(\tau)$ is finite at all τ, depends on the properties of a medium and defines the frequency-dependent dielectric permittivity

$$\varepsilon(\omega) = 1 + \int_0^\infty f(\tau)e^{i\omega\tau}d\tau. \tag{12}$$

6

Equations (11) and (12) constitute the mathematical formulation of the principle of causality stating that future has no effect on the past. From Eq. (12) it is seen that in the upper half-plane ($\text{Im}\,\omega > 0$) the integral converges and, thus, $\varepsilon(\omega)$ has no singular points [46]. This statement is a consequence of the principle of causality. It is easily seen also that in the upper half-plane (including the real frequency axis) the dielectric permittivity cannot turn into zero [46]. All the above results in the Kramers-Kronig relations which link to one another the real and imaginary parts of the dielectric permittivity.

From Fig. 1 and related discussion it is seen that the dielectric permittivity of the Gurzhi model does not satisfy the principle of causality and the Kramers-Kronig relations. Several attempts to recover the Kramers-Kronig relations have been undertaken (see, for instance, Refs. [36, 42, 47]) by introducing the so-called *memory function*, but its explicit form remains unavailable. In fact to cancel the first order pole at the point $i\xi^{(1)}$ in the upper half-plane of complex frequencies it would be necessary to replace the plasma frequency squared in Eq. (9) with the frequency- and temperature-dependent quantity

$$\tilde{\omega}_p^2(\omega, T) = \left[2iB\omega + 1 + \sqrt{1 + 4BC(T)}\right] g(\omega)\omega_p^2, \tag{13}$$

where $g(\omega)$ is any analytic function in the upper half-plane. In this case, however, the physically meaningful term of the order of ω^2 in Eq. (4) would be lost.

Thus, one can conclude that the Gurzhi model can be used only in some restricted region of low frequencies as more or less good phenomenological description for the dielectric permittivity of noble metals. In this respect it would be interesting to compare it with other analytic models used in computations of the Casimir force and with the experimental permittivity obtained from the measured optical data.

III. DIFFERENT MODELS OF THE DIELECTRIC PERMITTIVITY AND THE OPTICAL DATA

It is well known that the Lifshits formulas for the Casimir free energy and pressure are most conveniently expressed via the dielectric permittivity of plate materials along the imaginary frequency axis. The latter quantity, in its turn, can be found by means of the Kramers-Kronig relations

$$\varepsilon(i\xi) = 1 + \frac{2}{\pi} \int_0^\infty \frac{\omega\,\text{Im}\varepsilon(\omega)}{\omega^2 + \xi^2} d\omega \tag{14}$$

or

$$\varepsilon(i\xi) = 1 + \frac{2}{\pi} \int_0^\infty \frac{\omega \, \mathrm{Im}\varepsilon(\omega)}{\omega^2 + \xi^2} d\omega + \frac{\omega_p^2}{\xi^2} \tag{15}$$

expressing $\varepsilon(i\xi)$ through the imaginary part of ε defined along the real frequency axis. Equation (14) is valid for the permittivities that are regular at zero frequency or have a first order pole [8, 46], whereas Eq. (15) is obeyed by the permittivities having a second order pole and the residue ω_p^2 at zero frequency [8, 48].

Here we compare the imaginary parts of the dielectric permittivities of Au found from the measured optical data [9] and given by the Drude and Gurzhi models in the frequency region below 2 eV, i.e., well below the first absorption frequency.

In Figs. 2(a) and 2(b) the imaginary part of the dielectric permittivity of Au is shown by dots using the values for real and imaginary parts of the complex index of refraction of Au measured at frequencies above 0.125 eV [9]. The solid and dashed lines demonstrate the imaginary part of the dielectric permittivity of Au given by the Gurzhi (2) and Drude (1) models, respectively. In Fig. 2(a) the experimental values of parameters $\hbar\omega_p = 8.68$ eV and $\hbar\gamma_{ep}(T = 295\,\mathrm{K}) = 30.3$ meV [41] have been used. These parameters, however, are sample-dependent [22]. Because of this, in Fig. 2(b) $\mathrm{Im}\varepsilon$ given by the Gurzhi and Drude models are plotted using the values $\hbar\omega_p = 9.0$ eV and $\hbar\gamma_{ep}(T = 295\,\mathrm{K}) = 35.0$ meV which were found most appropriate for Au films employed in precise measurements of the Casimir force [11–21, 27].

As is seen in both Figs. 2(a) and 2(b), the Gurzhi model better reproduces the optical data than the Drude model over the frequency region from 0.3 to 2 eV. From the comparison of Fig. 2(a) and Fig. 2(b) it is seen also that the values of ω_p and γ used in experiments on measuring the Casimir force result in a better agreement between $\mathrm{Im}\varepsilon$ obtained from the optical data and from the Gurzhi and Drude models than the values of Ref. [41]. This result is readily illustrated by comparing insets in Figs. 2(a) and 2(b) where the frequency regions from 0.06 to 0.2 eV are shown on an enlarged scale. From the inset in Fig. 2(a) one can see that there is a break of continuity between the values of $\mathrm{Im}\varepsilon$ found from the optical data at the minimum frequency, where they are available, and from the analytic models. By contrast, in the inset to Fig. 2(b) there is a smooth extrapolation of the optical data by the Gurzhi and Drude models in the frequency region from 0 to 0.125 eV.

As mentioned in Sec. I, one of the approaches to the calculation of the Casimir force consists in using the optical data for $\mathrm{Im}\varepsilon$ over the entire frequency range where they are

available (from 0.125 to 9919 eV), extrapolated to below 0.125 eV (i.e., in the region from 0 to 0.125 eV) by means of the imaginary part of the Drude model [i.e., by the dashed line in Fig. 2(b)]. In doing so the values of $\varepsilon(i\xi)$ are obtained from Eq. (14) (there is no need in extrapolation of the optical data to the region above 9919 eV). This is the so-called Drude model approach to calculating the Casimir force which takes into account all real processes involving conduction and core electrons at frequencies above 0.125 eV and the electron-phonon interaction occurring at lower frequencies.

Another approach to calculate the Casimir force uses Imε determined by the optical data of Au only over the frequency range from 2 to 9919 eV related to interband transitions. It is assumed that Im$\varepsilon = 0$ within the frequency region from 0 to 2 eV, i.e., all the processes involving conduction electrons are disregarded. It is assumed also that the dielectric permittivity has a pole of second order and a residue equal to ω_p^2 at zero frequency. Then, the dielectric permittivity along the imaginary frequency axis is found from Eq. (15). This is called the plasma model approach to the calculation of the Casimir force. As described in Sec. I, the Casimir puzzle lies in the fact that all precise experiments on measuring the Casimir force at separations below 1 μm exclude the Drude model approach considered, and are in good agreement with the plasma model one (see also Sec. IV).

In the frequency region, where the Gurzhi dielectric permittivity is in reasonably good agreement with the optical data (i.e., below 2 eV), it could also be applied for calculating the Casimir force. For this purpose, at $\hbar\omega > 2$ eV Imε is obtained from the optical data and at $\hbar\omega < 2$ eV it is given by the imaginary part of the Gurzhi model. Then the dielectric permittivity along the entire imaginary frequency axis is found from Eq. (14). This could be called the Gurzhi model approach to the Casimir force. In the frequency region from 0.125 to 2 eV it takes into account analytically both the electron-phonon and electron-electron interactions (taken into account via the optical data in the Drude model approach). Both these processes are accounted for also at $\hbar\omega < 0.125$ eV [see the solid line in Fig. 2(b)], whereas the Drude model approach disregards the electron-electron scattering within this frequency region.

In the end of this section, we particularly emphasize that the type of singularity of ε at zero frequency makes a profound effect on its values at pure imaginary frequencies. As shown in Ref. [49], the behavior of $\varepsilon(i\xi)$ over the entire axis $0 < \xi < \infty$ can be found theoretically using the available optical data for the complex index of refraction with no any

extrapolation. This is achieved through the application of the so-called weighted Kramers-Kronig transform, which suppresses a contribution of the frequency regions where the optical data are not available, and assumes the presence of either the first or the second order pole of ε at zero frequency.

IV. CALCULATION OF THE CASIMIR PRESSURE IN DIFFERENT APPROACHES AND COMPARISON WITH EXPERIMENTS

The Casimir pressure between two parallel metallic plates of more than 100 nm thickness at temperature T separated by the vacuum gap of width a is the same as between two semispaces. It is given by the Lifshitz formula [1–5, 8]

$$P(a, T) = -\frac{k_B T}{\pi} \sum_{l=0}^{\infty}{}' \int_0^{\infty} q_l k_{\perp} dk_{\perp}$$
$$\times \sum_{\alpha} \left[r_{\alpha}^{-2}(i\xi_l, k_{\perp}) e^{2a q_l} - 1 \right]^{-1}, \tag{16}$$

where the prime on the first summation sign corresponds to dividing the term with $l = 0$ by 2, $k_{\perp}$ is the magnitude of projection of the wave vector on the plane of plates, α implies a summation over the transverse magnetic ($\alpha = $ TM) and transverse electric ($\alpha = $ TE) polarizations of the electromagnetic field, $\xi_l = 2\pi k_B T l/\hbar$ with $l = 0$, 1, 2, ... are the Matsubara frequencies, and $q_l = (k_{\perp}^2 + \xi_l^2/c^2)^{1/2}$.

The reflection coefficients in Eq. (16) are defined as

$$r_{\rm TM}(i\xi_l, k_{\perp}) = \frac{\varepsilon_l q_l - k_l}{\varepsilon_l q_l + k_l}, \quad r_{\rm TE}(i\xi_l, k_{\perp}) = \frac{q_l - k_l}{q_l + k_l}, \tag{17}$$

where

$$\varepsilon_l \equiv \varepsilon(i\xi_l), \quad k_l = \left(k_{\perp}^2 + \varepsilon_l \frac{\xi_l^2}{c^2} \right)^{1/2}. \tag{18}$$

From Eq. (4) it is seen that at the first Matsubara frequency it holds $\gamma_{ee}(i\xi_1, T) = 0$. This is the so-called *first-Matsubara-frequency* rule [38].

We have calculated the ratio of the Casimir pressure (16) at $T = 295$ K to that between two ideal metal plates at zero temperature, $P_0(a) = -\pi^2 \hbar c/(240 a^4)$, as a function of separation between the plates, using three theoretical approaches described in the end of Sec. III, i.e., the plasma, Drude, and Gurzhi. The computational results are presented in Fig. 3 by the three solid lines counted from top to bottom. These lines are obtained by using extrapolations of the optical data to below 2 eV by means of the plasma model with $\hbar\omega_p = 9.0$ eV,

to below 0.125 eV by means of the Drude model with $\hbar\omega_p = 9.0$ eV, $\hbar\gamma_{ep} = 35$ meV, and to below 2 eV by means of the Gurzhi model with $\hbar\omega_p = 8.68$ eV, $\hbar\gamma_{ep}(T = 295\,\text{K}) = 30.3$ meV, respectively. The dashed line is found by extrapolating the optical data to below 2 eV using the Gurzhi model with $\hbar\omega_p = 9.0$ eV and $\hbar\gamma_{ep} = 35$ meV.

As is seen in Fig. 3, the Drude and Gurzhi approaches lead to rather close results for the Casimir pressure, especially if the Gurzhi model employs the same Drude parameters as the Drude model (see the dashed line). At the same time, the computational results found within the plasma model approach are quite different. This is explained by distinct behaviors of the dielectric permittivities at zero frequency (the first order pole in the cases of Drude and Gurzhi models and the second order one for the plasma model).

To quantify the role of the optical data below 2 eV and at higher frequencies in the region of absorption bands, in Table I we present several computational results found with the partial or total exclusion of the use of optical data in favor of the simple plasma or Drude models. Columns 3, 5, and 8 of Table I contain magnitudes of the Casimir pressure computed using the plasma, Drude and Gurzhi model approaches, respectively, at separation distances indicated in column 1. These computations are performed with the optical data, as described in explanations to Fig. 3, with the Drude parameters $\hbar\omega_p = 9.0$ eV and $\hbar\gamma_{ep} = 35$ meV. In column 2 of Table I, we present the mean measured magnitudes of the Casimir pressure and their total experimental errors determined at the 95% confidence level by the results of Refs. [13, 14]. In columns 4 and 7, the magnitudes of the Casimir pressure computed by using the simple plasma and Drude models are presented, respectively, i.e.,

$$\varepsilon_p(i\xi_l) = 1 + \frac{\omega_p^2}{\xi_l^2}, \quad \varepsilon_D(i\xi_l) = 1 + \frac{\omega_p^2}{\xi_l[\xi_l + \gamma_{ep}(T)]}. \tag{19}$$

Finally, column 6 contains the computational results using the optical data of Au at $\hbar\omega > 2$ eV and the simple Drude model at $\hbar\omega \leq 2$ eV.

We note that computations of the Casimir pressure by using the simple Gurzhi model (2) applied over the entire frequency range would be inconsistent. The reason is that in the region from $\hbar\xi^{(1)} = 63.3217$ eV to $\hbar\xi^{(0)} = 64.47$ eV one has $\varepsilon_G(i\xi) < 0$ (see Sec. II). The width of the frequency interval where $\varepsilon_G(i\xi)$ is negative is almost independent of the values of the Drude parameters. For instance, for $\hbar\omega_p = 9.0$ eV and $\hbar\gamma_{ep} = 35$ meV it holds $\hbar\xi^{(1)} = 63.3261$ eV in place of 63.3217 eV. As a result, at room temperature ($T = 295$ K) one obtains that $\varepsilon_G(i\xi_l)$ with $397 \leq l \leq 403$ takes the negative values. This leads to the

11

complex k_l in Eq. (18) within some interval of $k_\perp$ and, finally, to the complex reflection coefficients and Casimir pressures in Eq. (16).

It may be argued that the Matsubara terms with such high l do not contribute to the pressure at separations considered. The presence of the complex-valued terms (even though they were negligibly small in magnitudes) is, however, quite impermissible theoretically. Furthermore, at sufficiently short separations between the plates it is necessary to take into account much larger number of Matsubara terms in order to calculate the Casimir pressure with sufficient precision. Usually one should include all terms up to $15\omega_c = 15c/(2a)$ [8]. As a result, at $a = 15$ nm the first 650 Matsubara terms should be included at room temperature. This makes apparent that the simple Gurzhi model cannot be used over the entire frequency range not only theoretically but from the practical standpoint as well.

Now we discuss a correlation between the magnitudes of the Casimir pressure in columns 3–8 of Table I. We note that these values are burdened by the errors of approximately 0.5% determined by inaccuracies in the optical data and values of parameters in the models used [8]. An interrelationship between the values in columns 3, 5, and 8 (obtained using the plasma, Drude, and Gurzhi approaches, respectively) is the same as already discussed above for respective lines in Fig. 3. By comparing column 4 with column 3, it is seen that the use of the simple plasma model (column 4) results in slightly smaller magnitudes of the Casimir pressure, and the impact of the optical data becomes more pronounced with decreasing separation between the plates.

If one uses the simple Drude model at all frequencies below 2 eV (column 6), slightly smaller magnitudes of the Casimir pressure are obtained as compared to column 5, where the optical data are extrapolated down to zero frequency by the simple Drude model in the region $\hbar\omega < 0.125$ eV. When the simple Drude model is applied over the entire frequency axis (column 7), even smaller values for the magnitudes of the Casimir pressure are obtained. With increasing separation, however, differences between the Casimir pressures in columns 5, 6, and 7 become negligibly small which reflects a decreasing impact of the optical data in the region of absorption bands on the computational results. Note also that the Gurzhi model approach to calculation of the Casimir force (column 8) leads to almost the same (but slightly larger) pressure magnitudes as those in column 6 obtained using the simple Drude model below 2 eV and the optical data at all higher frequencies.

A comparison between the Casimir pressures found with the Gurzhi model approach

(column 8) and by means of the Drude model below 2 eV (column 6) allows estimation of the role of electron-electron scattering in the Casimir interaction. At $a = 0.2\,\mu$m it contributes only about 0.16% of the pressure and its contribution decreases with increasing separation.

By comparing the experimental Casimir pressures in column 2 with the theoretical ones in columns 3–8 one can conclude that in the limits of experimental and theoretical errors the measurement data are in agreement with the theoretical predictions made using the plasma model approach and exclude the predictions of all other approaches. This conclusion can be made quantitative taking into account that all precise experiments on measuring the Casimir interaction have been performed in the sphere-plate geometry (rather than in the plate-plate one) and that the test bodies have some surface roughness, which is not taken into account in the theoretical results of columns 3–8.

In the experiment of Refs. [13, 14], performed by means of a micromechanical oscillator, the immediately measured quantity was the gradient of the Casimir force acting between the sphere of $R = 150\,\mu$m radius and a plate. This quantity can be recalculated in the magnitude of the Casimir pressure between two parallel plates presented in column 2 of Table I using the proximity force approximation [1, 8]

$$|P(a,T)| = \frac{1}{2\pi R}\frac{\partial F_{sp}(a,T)}{\partial a}. \tag{20}$$

The relative corrections to an approximate expression (20), which are less than a/R [24, 25], are negligibly small in this experiment. Small corrections due to the surface roughness have been taken into account perturbatively [1, 8, 50] in the Casimir pressure P_{theor} (note that the surface roughness plays a more important role at very short separations between the test bodies [51]).

In Fig. 4, we plot the differences between the theoretical Casimir pressures computed using the plasma, Drude and Gurzhi model approaches and mean experimental pressures measured in Refs. [13, 14] (three sets of dots counted from bottom to top, respectively) as the functions of separation. The Drude parameters in the Gurzhi model are chosen as (a) $\hbar\omega_p = 8.68\,$eV and $\hbar\gamma_{ep} = 30.3\,$meV and (b) $\hbar\omega_p = 9.0\,$eV and $\hbar\gamma_{ep} = 35\,$meV. The solid lines are formed by the borders of the confidence intervals found at each separation by combining the total experimental and theoretical errors determined at the 95% confidence probability. As is seen in Figs. 4(a) and 4(b), both the Drude model approach and the Gurzhi model

13

one used with any set of the Drude parameters are excluded by the measurement data at the 95% confidence level, whereas the plasma model approach is experimentally consistent.

We also compare the theoretical predictions of all three approaches with the recently measured gradient of the Casimir force acting between the Au-coated surfaces of a sphere and a plate refined by means of the UV and Ar-ion cleaning [20]. In this work, performed by means of an atomic force microscope, the sphere radius was reduced to $R = 43\ \mu$m, and the corrections due to the use of the proximity force approximation have been taken into account through the results of Ref. [25]. The corrections due to the surface roughness were also included in the theoretical gradients of the Casimir force [20].

In Fig. 5 the differences between the theoretical gradients of the Casimir force computed within the plasma, Drude and Gurzhi model approaches and mean experimental gradients [20] (the sets of dots counted from top to bottom, respectively) are shown as the functions of separation. The Drude parameters in the Gurzhi model are again chosen as (a) $\hbar\omega_p = 8.68$ eV and $\hbar\gamma_{ep} = 30.3$ meV and (b) $\hbar\omega_p = 9.0$ eV and $\hbar\gamma_{ep} = 35$ meV. The solid lines indicate the borders of the confidence intervals determined in this experiment at the 67% confidence probability by combining the total experimental and theoretical errors. From Figs. 5(a) and 5(b) it is seen that both the Drude model approach and the Gurzhi model approach are excluded by the measurement data which are consistent with the plasma model approach to calculation of the Casimir force.

V. CONCLUSIONS AND DISCUSSION

In the foregoing, we have discussed the extended Drude model or, as it also named, the Gurzhi model, which describes the relaxation properties of conduction electrons originating from electron-phonon and electron-electron scattering. Although this model is often used in condensed matter physics and, specifically, in the theory of high-temperature superconductors, its applications in the theory of Casimir forces were not considered so far. Taking into account that the Casimir puzzle remains unsolved for already 20 years (see Sec. I), investigation of possible extensions of the Drude model in connection with the Lifshitz theory is a subject of much current interest.

We have considered the analytic properties of the dielectric permittivity of the Gurzhi model. It is shown that this permittivity has a first order pole in the upper half-plane of

complex frequencies and, thus, violates the causality principle. Additionally, within some interval along the pure imaginary frequency axis, the Gurzhi dielectric permittivity takes the negative values. One thus concludes that for calculating the Casimir force it can be used only in the frequency region below the absorption bands of a metal in combination with the dielectric permittivity obtained from the measured optical data at higher frequencies.

Next, we have considered the imaginary part of the dielectric permittivity of the Gurzhi model for Au at frequencies below 2 eV which can be used to calculate the Casimir pressure by means of the Lifshitz formula. It was found to be in closer agreement with $\text{Im}\varepsilon$ defined from the optical data and it leads to almost the same, as the Drude model, extrapolation down to zero frequency, i.e., to the region where the optical data are not available. The concept of the Gurzhi model approach to the Casimir force is introduced by analogy with the Drude and plasma model approaches using the respective models combined with the optical data. As discussed in Sec. I, the two latter approaches are the subject of a considerable literature in connection with the Casimir puzzle.

The Casimir pressure between two Au plates was calculated using the Drude, plasma and Gurzhi model approaches, as well as by using the simple Drude and plasma models, and also by means of the Drude model applied in the region from zero frequency to 2 eV and supplemented by the optical data at higher frequencies. The obtained results are compared with the data of two precise experiments on measuring the Casimir interaction. The contribution of electron-electron interaction to the Casimir force is estimated to be less than 0.16%. The Gurzhi model approach is shown to be excluded by the measurement data, as it was demonstrated earlier for the Drude model approach. An agreement of the plasma model approach with the measurement data at separations below 1 μm is confirmed.

Although the above results do not solve the Casimir puzzle, they attach special significance to novel experiments on measuring the Casimir force in the micrometer separation range proposed in Refs. [52–54].

---

[1] G. L. Klimchitskaya, U. Mohideen, and V. M. Mostepanenko, The Casimir force between real materials: Experiment and theory, Rev. Mod. Phys. **81**, 1827 (2009).

[2] A. W. Rodrigues, F. Capasso, and S. G. Johnson, The Casimir effect in microstructured geometries, Nat. Photon. **5**, 211 (2011).

[3] L. M. Woods, D. A. R. Dalvit, A. Tkatchenko, P. Rodriguez-Lopez, A. W. Rodriguez, and R. Podgornik, Materials perspective on Casimir and van der Waals interactions, Rev. Mod. Phys. **88**, 045003 (2016).

[4] E. M. Lifshitz, The theory of molecular attractive forces between solids, Zh. Eksp. Teor. Fiz. **29**, 94 (1955) [Sov. Phys. JETP **2**, 73 (1956)].

[5] I. E. Dzyaloshinskii, E. M. Lifshitz, and L. P. Pitaevskii, The general theory of van der Waals forces, Usp. Fiz. Nauk **73**, 381 (1961) [Adv. Phys. **10**, 165 (1961)].

[6] J. S. Høye and I. Brevik, Van der Waals force between dielectric plates derived from the quantum statistical mechanical path integral method, Physica A (Amsterdam) **259**, 165 (1998).

[7] S. J. Rahi, T. Emig, N. Graham, R. L. Jaffe, and M. Kardar, Scattering theory approach to electrodynamic Casimir forces, Phys. Rev. D **80**, 085021 (2009).

[8] M. Bordag, G. L. Klimchitskaya, U. Mohideen, and V. M. Mostepanenko, *Advances in the Casimir Effect* (Oxford University Press, Oxford, 2015).

[9] *Handbook of Optical Constants of Solids*, ed. E. D. Palik (Academic, New York, 1985).

[10] J. S. Høye and I. Brevik, Casimir force between a half-space and a plate of finite thickness, Phys. Rev. A **93**, 052504 (2016).

[11] R. S. Decca, E. Fischbach, G. L. Klimchitskaya, D. E. Krause, D. López, and V. M. Mostepanenko, Improved tests of extra-dimensional physics and thermal quantum field theory from new Casimir force measurements, Phys. Rev. D **68**, 116003 (2003).

[12] R. S. Decca, D. López, E. Fischbach, G. L. Klimchitskaya, D. E. Krause, and V. M. Mostepanenko, Precise comparison of theory and new experiment for the Casimir force leads to stronger constraints on thermal quantum effects and long-range interactions, Ann. Phys. (N.Y.) **318**,

37 (2005).

[13] R. S. Decca, D. López, E. Fischbach, G. L. Klimchitskaya, D. E. Krause, and V. M. Mostepanenko, Tests of new physics from precise measurements of the Casimir pressure between two gold-coated plates, Phys. Rev. D **75**, 077101 (2007).

[14] R. S. Decca, D. López, E. Fischbach, G. L. Klimchitskaya, D. E. Krause, and V. M. Mostepanenko, Novel constraints on light elementary particles and extra-dimensional physics from the Casimir effect, Eur. Phys. J. C **51**, 963 (2007).

[15] C.-C. Chang, A. A. Banishev, R. Castillo-Garza, G. L. Klimchitskaya, V. M. Mostepanenko, and U. Mohideen, Gradient of the Casimir force between Au surfaces of a sphere and a plate measured using an atomic force microscope in a frequency-shift technique, Phys. Rev. B **85**, 165443 (2012).

[16] A. A. Banishev, C.-C. Chang, G. L. Klimchitskaya, V. M. Mostepanenko, and U. Mohideen, Measurement of the gradient of the Casimir force between a nonmagnetic gold sphere and a magnetic nickel plate, Phys. Rev. B **85**, 195422 (2012).

[17] A. A. Banishev, G. L. Klimchitskaya, V. M. Mostepanenko, and U. Mohideen, Demonstration of the Casimir Force between Ferromagnetic Surfaces of a Ni-Coated Sphere and a Ni-Coated Plate, Phys. Rev. Lett. **110**, 137401 (2013).

[18] A. A. Banishev, G. L. Klimchitskaya, V. M. Mostepanenko, and U. Mohideen, Casimir interaction between two magnetic metals in comparison with nonmagnetic test bodies, Phys. Rev. B **88**, 155410 (2013).

[19] J. Xu, G. L. Klimchitskaya, V. M. Mostepanenko, and U. Mohideen, Reducing detrimental electrostatic effects in Casimir-force measurements and Casimir-force-based microdevices, Phys. Rev. A **97**, 032501 (2018).

[20] M. Liu, J. Xu, G. L. Klimchitskaya, V. M. Mostepanenko, and U. Mohideen, Examining the Casimir puzzle with an upgraded AFM-based technique and advanced surface cleaning, Phys. Rev. B **100**, 081406(R) (2019).

[21] M. Liu, Jun Xu, G. L. Klimchitskaya, V. M. Mostepanenko, and U. Mohideen, Precision measurements of the gradient of the Casimir force between ultraclean metallic surfaces at larger separations, Phys. Rev. A **100**, 052511 (2019).

[22] V. B. Svetovoy, P. J. van Zwol, G. Palasantzas, and J. Th. M. De Hosson, Optical properties of gold films and the Casimir force, Phys. Rev. B **77**, 035439 (2008).

[23] R. O. Behunin, D. A. R. Dalvit, R. S. Decca, C. Genet, I. W. Jung, A. Lambrecht, A. Liscio, D. López, S. Reynaud, G. Schnoering, G. Voisin, and Y. Zeng, Kelvin probe force microscopy of metallic surfaces used in Casimir force measurements, Phys. Rev. A **90**, 062115 (2014).

[24] G. Bimonte, T. Emig, R. L. Jaffe, and M. Kardar, Casimir forces beyond the proximity force approximation, Europhys. Lett. **97**, 50001 (2012).

[25] M. Hartmann, G.-L. Ingold, and P. A. Maia Neto, Plasma versus Drude Modeling of the Casimir Force: Beyond the Proximity Force Approximation, Phys. Rev. Lett. **119**, 043901 (2017).

[26] G. Bimonte, Hide to See It Better: A Robust Setup to Probe the Thermal Casimir Effect, Phys. Rev. Lett. **112**, 240401 (2014).

[27] G. Bimonte, D. López, and R. S. Decca, Isoelectronic determination of the thermal Casimir force, Phys. Rev. B **93**, 184434 (2016).

[28] G. L. Klimchitskaya and V. M. Mostepanenko, Experiment and theory in the Casimir effect, Contemp. Phys. **47**, 131 (2006).

[29] M. Boström and Bo E. Sernelius, Thermal Effects on the Casimir Force in the 0.1-5μm Range, Phys. Rev. Lett. **84**, 4757 (2000).

[30] A. O. Sushkov, W. J. Kim, D. A. R. Dalvit, and S. K. Lamoreaux, Observation of the thermal Casimir force, Nature Physics **7**, 230 (2011).

[31] G. L. Klimchitskaya, M. Bordag, and V. M. Mostepanenko, Comparison between experiment and theory for the thermal Casimir force, Int. J. Mod. Phys. A **27**, 1260012 (2012).

[32] V. B. Bezerra, G. L. Klimchitskaya, U. Mohideen, V. M. Mostepanenko, and C. Romero, Impact of surface imperfections on the Casimir force for lenses of centimeter-size curvature radii, Phys. Rev. B **83**, 075417 (2011).

[33] I. Brevik and J. S. Høye, Temperature dependence of the Casimir force, Eur. J. Phys. **35**, 015012 (2014).

[34] *Casimir Physics*, eds. D. A. R. Dalvit, P. Milonni, R. Roberts, and F. da Rosa (Springer, Berlin, 2013).

[35] W. M. R. Simpson and U. Leonhardt, *Force of the Quantum Vacuum: An Introduction to Casimir Physics* (World Scientific, Singapore, 2015).

[36] D. N. Basov, R. D. Averitt, D. van der Marel, M. Dressel, and K. Haule, Electrodynamics of correlated electron materials, Rev. Mod. Phys. **83**, 471 (2011).

[37] L. P. Pitaevskii, The anomalous skin effect in the infra-red region, Zh. Eksp. Teor. Fiz. **34**, 942 (1958) [Sov. Phys. JETP **34**, 652 (1958)].

[38] D. L. Maslov and A. V. Chubukov, Optical response of correlated electron systems, Rep. Progr. Phys. **80**, 026503 (2017).

[39] R. N. Gurzhi, Mutual electron correlations in metal optics, Zh. Eksp. Teor. Fiz. **35**, 965 (1958) [Sov. Phys. JETP **35**, 673 (1959)].

[40] R. T. Beach and R. W. Christy, Electron-electron scattering in the intraband optical conductivity of Cu, Ag, and Au, Phys. Rev. B **16**, 5277 (1977).

[41] G. R. Parkins, W. E. Lawrence, and R. W. Christy, Intraband optical conductivity $\sigma(\omega, T)$ of Cu, Ag, and Au: Contribution from electron-electron scattering, Phys. Rev. B **23**, 6408 (1981).

[42] S. J. Youn, T. H. Rho, B. I. Min, and K. S. Kim, Extended Drude model analysis of noble metals, Physica Status Solidi (b) **244**, 1354 (2007).

[43] R. L. Olmon, B. Slovick, T. W. Johnson, D. Shelton, S.-H. Oh, G. D. Boreman, and M. B. Raschke, Optical dielectric function of gold, Phys. Rev. B **86**, 235147 (2012).

[44] H. U. Yang, J. D'Archangel, M. L. Sundheimer, E. Tucker, G. D. Boreman, and M. B. Raschke, Optical dielectric function of silver, Phys. Rev. B **91**, 235137 (2015).

[45] M. Xu, J.-Y. Yang, S. Zhang, and L. Liu, Role of electron-phonon coupling in finite-temperature dielectric functions of Au, Ag, and Cu, Phys. Rev. B **96**, 115154 (2017).

[46] L. D. Landau, E. M. Lifshitz, and L. P. Pitaevskii, *Electrodynamics of Continuous Media* (Pergamon, Oxford, 1984).

[47] A. V. Puchkov, D. N. Basov, and T. Timusk, The pseudogap state in high-T_c superconductors: an infrared study, J. Phys.: Condens. Matter **8**, 10049 (1996).

[48] G. L. Klimchitskaya, U. Mohideen, and V. M. Mostepanenko, Kramers-Kronig relations for plasma-like permittivities and the Casimir force, J. Phys. A: Math. Theor. **40**, 339 (2007).

[49] G. Bimonte, Making precise predictions of the Casimir force between metallic plates via a weighted Kramers-Kronig transform, Phys. Rev. A **83**, 042109 (2011).

[50] M. Bordag, G. L. Klimchitskaya, and V. M. Mostepanenko, The Casimir force between plates with small deviations from plane parallel geometry, Int. J. Mod. Phys. A **10**, 2661 (1995).

[51] W. Broer, G. Palasantzas, J. Knoester, and V. B. Svetovoy, Roughness correction to the Casimir force at short separations: Contact distance and extreme value statistics, Phys. Rev.

B **85**, 155410 (2012).

[52] G. Bimonte, G. L. Klimchitskaya, and V. M. Mostepanenko, Universal experimental test for the role of free charge carriers in the thermal Casimir effect within a micrometer separation range, Phys. Rev. A **95**, 052508 (2017).

[53] G. Bimonte, Apparatus to probe the influence of the Mott-Andersen metal-insulator transition in doped semiconductors on the Casimir effect, Phys. Rev. A **99**, 052506 (2019).

[54] G. L. Klimchitskaya, V. M. Mostepanenko, and R. I. P. Sedmik, Casimir pressure between metallic plates out of thermal equilibrium: Proposed test for the relaxation properties of free electrons, Phys. Rev. A **100**, 022511 (2019).

TABLE I: Magnitudes of the mean measured Casimir pressure [13, 14] (column 2) at $T = 295$ K at different separations (column 1) are compared with the magnitudes of theoretical pressures computed using the plasma model approach (column 3), the simple plasma model (column 4), the Drude model approach (column 5), the Drude model used below the first absorption band (column 6), the simple Drude model (column 7), and the Gurzhi model approach (column 8). In all cases the Drude parameters $\hbar\omega_p = 9.0$ eV and $\hbar\gamma_{ep} = 35$ meV have been used.

|	$|P|$ (mPa)						
a (μm)	2	3	4	5	6	7	8
0.2	510.5 ± 1.0	512.19	501.82	497.35	493.80	483.29	494.57
0.3	114.8 ± 0.5	115.02	114.04	109.69	109.14	108.13	109.25
0.4	39.2 ± 0.4	39.15	38.98	36.70	36.57	36.39	36.59
0.5	16.8 ± 0.4	16.81	16.76	15.50	15.45	15.41	15.46
0.6	8.4 ± 0.4	8.38	8.36	7.60	7.579	7.565	7.582
0.7	4.7 ± 0.4	4.632	4.628	4.132	4.124	4.119	4.125
0.8		2.767	2.765	2.427	2.423	2.421	2.424
0.9		1.754	1.753	1.512	1.5103	1.5092	1.5105
1.0		1.165	1.164	0.9874	0.9864	0.9859	0.9865
1.1		0.8041	0.8039	0.6699	0.6692	0.6690	0.6693
1.2		0.5730	0.5729	0.4690	0.4687	0.4635	0.4687
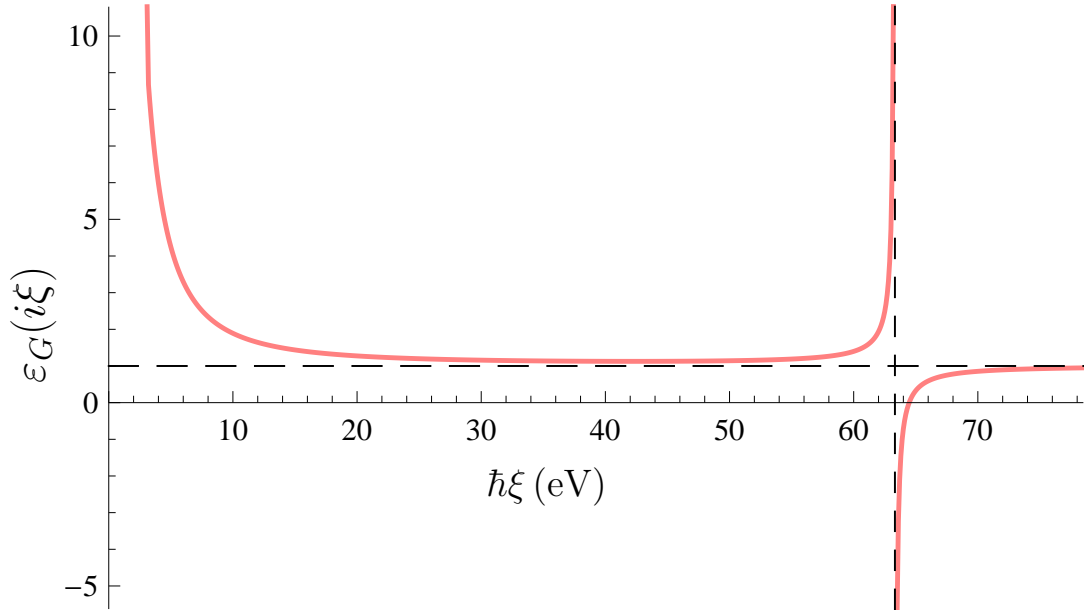
FIG. 1: The dielectric permittivity of the Gurzhi model is shown as a function of the imaginary frequency.
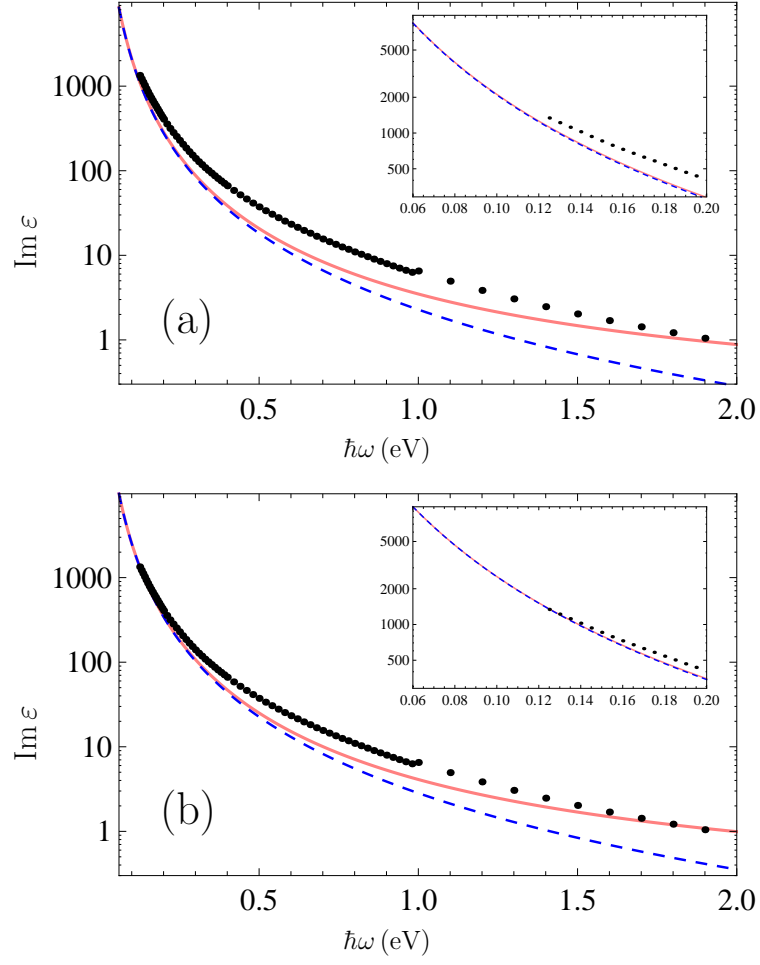
FIG. 2: The imaginary part of the dielectric permittivity of Au is shown as a function of frequency by the dots obtained from the optical data for the complex index of refraction and by the solid and dashed lines obtained using the Gurzhi and Drude models, respectively, with the plasma frequency and relaxation parameter (a) $\hbar\omega_p = 8.68$ eV, $\hbar\gamma_{ep} = 30.3$ meV and (b) $\hbar\omega_p = 9.0$ eV, $\hbar\gamma_{ep} = 35.0$ meV. The region of small frequencies is shown in the insets on an enlarged scale.
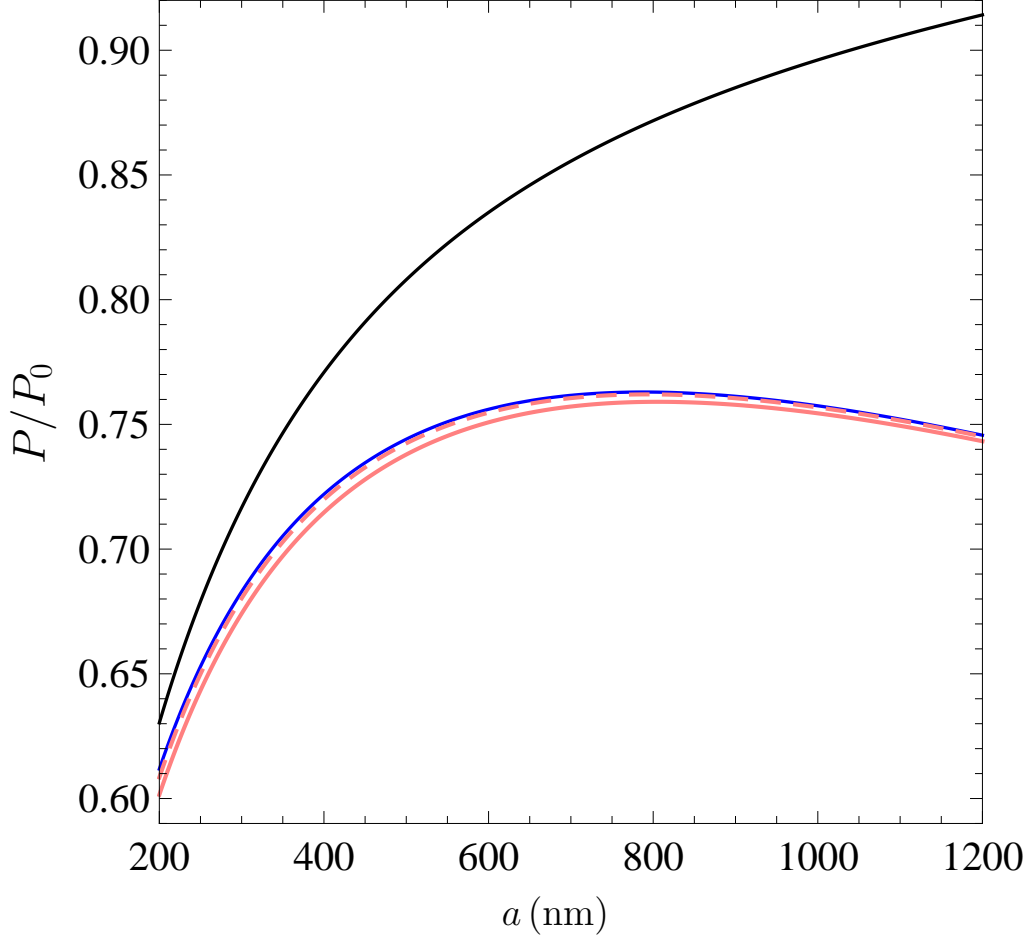
FIG. 3: The ratio of the Casimir pressure between two parallel Au plates obtained at $T = 295$ K using an extrapolation of the optical data in the region from 0 to 2 eV by means of the plasma model with $\hbar\omega_p = 9.0$ eV (the top solid line), in the region from 0 to 0.125 eV by means of the Drude model with $\hbar\omega_p = 9.0$ eV, $\hbar\gamma_{ep} = 35.0$ meV (the middle solid line), and in the region from 0 to 2 eV by means of the Gurzhi model with $\hbar\omega_p = 8.68$ eV, $\hbar\gamma_{ep} = 30.3$ meV (the bottom solid line) to the pressure between two ideal metal plates is shown as function of separation. The dashed line shows the same ratio where the numerator is calculated using the Gurzhi model with $\hbar\omega_p = 9.0$ eV and $\hbar\gamma_{ep} = 35.0$ meV.
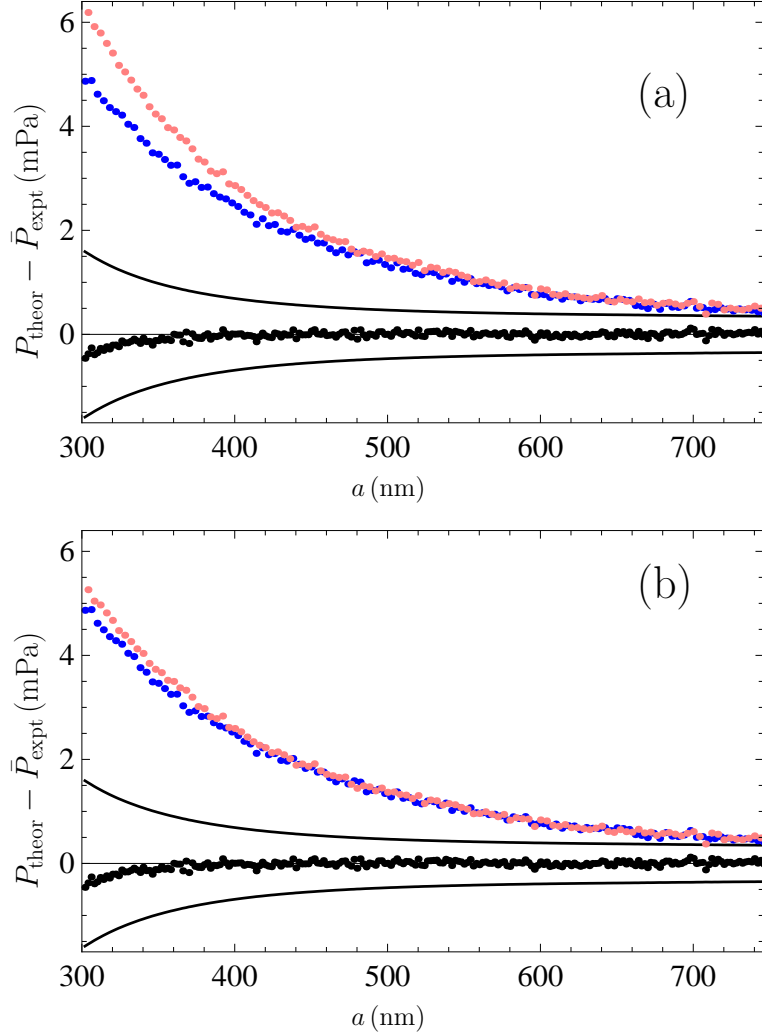
FIG. 4: The differences between theoretical and mean experimental [13, 14] Casimir pressures at $T = 295$ K computed using an extrapolation of the optical data of Au in the region from 0 to 2 eV by means of the plasma model with $\hbar\omega_p = 9.0$ eV (the bottom set of dots), in the region from 0 to 0.125 eV by means of the Drude model with $\hbar\omega_p = 9.0$ eV, $\hbar\gamma_{ep} = 35.0$ meV (the middle set of dots), and in the region from 0 to 2 eV by means of the Gurzhi model (the top set of dots) are shown as the functions of separation. The Drude parameters in the Gurzhi model are (a) $\hbar\omega_p = 8.68$ eV, $\hbar\gamma_{ep} = 30.3$ meV and (b) $\hbar\omega_p = 9.0$ eV, $\hbar\gamma_{ep} = 35.0$ meV. Two solid lines indicate the borders of the confidence intervals found at the 95% confidence probability.
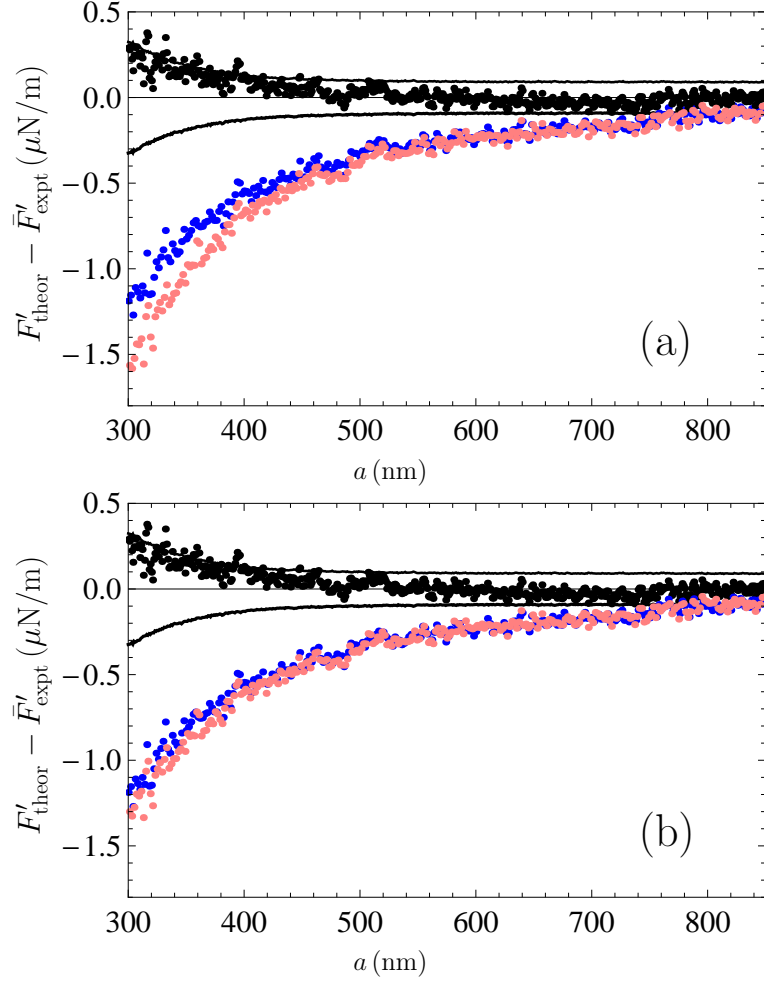
FIG. 5: The differences between theoretical and mean experimental [20] gradients of the Casimir force at $T = 295$ K computed using an extrapolation of the optical data of Au in the region from 0 to 2 eV by means of the plasma model with $\hbar\omega_p = 9.0$ eV (the top set of dots), in the region from 0 to 0.125 eV by means of the Drude model with $\hbar\omega_p = 9.0$ eV, $\hbar\gamma_{ep} = 35.0$ meV (the middle set of dots), and in the region from 0 to 2 eV by means of the Gurzhi model (the bottom set of dots) are shown as the functions of separation. The Drude parameters in the Gurzhi model are (a) $\hbar\omega_p = 8.68$ eV, $\hbar\gamma_{ep} = 30.3$ meV and (b) $\hbar\omega_p = 9.0$ eV, $\hbar\gamma_{ep} = 35.0$ meV. Two solid lines indicate the borders of the confidence intervals found at the 67% confidence probability.

26